The Effect of Nano-Alumina Particles Generated *in Situ* in the Matrix of Ultralow and No Cement 85 wt% Al₂O₃ Refractory Castables

José Antonio Alves Júnior, João Baptista Baldo

Department of Materials Engineering, Federal University of São Carlos via Washington Luis, São Carlos, SP, Brazil
Email: baldo@ufscar.br, jjunior8404@gmail.com

Abstract

Advanced high alumina refractory castables of ultra-low and to cement types, are well-known because of their ability on developing similar and/or superior thermal and mechanical properties. Following the recent trend of including nanoparticles in refractory castables, in this work, it is presented a novel way to obtain the benefit effects on the thermal and mechanical properties, promoted by the development *in situ*, of alumina's nanoparticles in the matrix of castable (85 wt% Al₂O₃). The alumina nanoparticles were originated *in situ* after firing, due to the pyrolysis and oxidation of an aqueous resin, produced by the Pechini process. The resin played a double role, one as mixing liquid vehicle and the other as the aluminum oxide nanoparticles precursor. The results indicate a strong increase in flexural strength and elastic modulus as well as leading to a higher residual strength after thermal shock.

Keywords

1. Introduction

Within the advanced monolithic refractory classes; the ultra-low (ULCC) and non-cement (NCC) refractory castables, display versatility and notable performance. Each one in its niche, occupy a prominent role in the refractories application universe [1] [2].

The advances in the technology of these monolithics were made possibly from the continuous decrease in the calcium aluminate cement (CAC) contents, the use of alternative binders such as of colloidal silica, colloidal alumina and Hy-

dratable Alumina (HA). These new binders, together with the inclusion of sub micrometric mineral admixtures, lead to particle packing optimization promoting collateral reactivity through the formation of other cementitious compounds and/or acting as sintering mineralizers. In addition, better rheological control of the mixes was accomplished by the inclusion of packages of special additives such, deflocullants, accelerators and retarders [1] [3].

It is a well-known fact that the macro and micro properties of all refractories, monolithics or not, are depended basically on the right combination of refractory phases and the resultant microstructure. In this sense, once the raw materials selection based on sinergistic preconditions is pacified with respect to the target application, the resultant monolithic matrix turns out to be one key microstructural element to determine the material's final performance.

Based on this premise, this work shows the positive effects on the mechanical and thermomechanical properties, promoted by the development *in situ* of alumina nanoparticles in the matrices of high alumina (≥ 85 wt% Al_2O_3) refractory castables, of the Ultra Low (3.0 wt% CAC) and No Cement (3.5 wt% HA) types.

Conversely to what has been reported in the literature [4] [5], a new methodology was used in this work, that is; instead of adding a colloidal suspension or a previously made nano alumina powder, the development of the alumina nanoparticles was done *in situ*, using as their precursor, an aqueous polymeric resin, produced by the Pechini method [6] [7]. In this specific resin, Al^{3+} cations were part of the polymeric chain. In doing so, the resin fulfilled a dual function of mixing water carrier as well as the precursor vehicle of nanoparticles of aluminum oxide, generated upon pyrolysis and oxidation of the aluminum cation of the resin back bone [2].

The rationale behind this procedure resides in the expected non-agglomerated more homogeneous distribution of the nanoparticles around the aggregates. Secondly, the nascent character of the *in situ* formed alumina nano particles, would provide a greater reactive potential with the other aggregates in the castable matrix, strengthening it [2] [3]. This was confirmed comparatively to the same castables base compositions using only water as the liquid vehicle, instead of the polymeric resin.

2. Materials and Methods

2.1. Ultralow and No Cement Refractory Specimens

Four sets of samples using the compositions shown in Table 1 were produced. The first set of the ultralow cement type used water as the mixing liquid and was named $ULCC_{water}$. The second set of the ultra-low cement type used the Al polymeric resin as mixing liquid and was named $ULCC_{Al_2O_3}$. The first set of the no cement type used water as the mixing liquid and was named NCC_{water}. The second set of no cement type used the Al polymeric resin as the mixing liquid and was named $NCC_{Al_2O_3}$.

Table 1. Weight Percentages of the raw materials used in the production of the investigated castables samples.

Composition	ULCC$_{water}$	ULCC$_{Al_2O_3}$	NCC$_{water}$	NCC$_{Al_2O_3}$
Elfusa White Fused Alumina AL 4/10	21%	21%	21%	21%
Elfusa White Fused Alumina AL 10/20	16%	16%	16%	16%
Elfusa White Fused Alumina AL 20/40	12%	12%	10%	10%
Elfusa White Fused Alumina AL 70/140	11%	11%	13%	13%
Elfusa White Fused Alumina AL-TPFII	18%	18%	18%	18%
Calcined Alumina CT3000	14.0%	14%	13%	13%
Hydratable Alumina (HA)[1]	-	-	3.5%	3.5%
Cement Secar 71	3.0%	3.0%	0.5%	0.5%
Elkem Microsilica – 971U	5%	5%	5.0%	5.0%
STP[2]	0.1%	0.1%	0.1%	0.1%
APA[3]	0.05%	0.05%	0.05%	0.05%
H$_2$O	5.5%	-	5.7%	-
Resin Al[4]	-	8.0%	-	8.0%

[1]Alphabond 300. [2]STP = Sodium Tripolyphosphate. [3]APA = Amonium Polyacrilate. [4]The quantity of 8 wt% of liquid polymeric resin was equivalent to the addition of 1 wt% of alumina nanoparticles after pyrolysis.

The compositions were devised to approximate an Andreasen's particle size packing with a distribution modulus q = 0.26, aiming an almost self flowing rheological condition.

2.2. Synthesis of the Polymeric Resin by the Pechini Method

The basics of the Pechini's methodology [6] to produce the polymeric resin, consists in the dissolution in deionized water at 70°C, of a salt of the cation of interest, in this case, Al(NO$_3$)$_3$. In the sequence, citric acid is added forming the metallic citrate. In order to promote the esterification reaction, ethylene glycol is added and the temperature is raised to 90°C, keeping the system for two hours under this condition. The resin viscosity can be controlled by evaporating the residual water simply expositing it at 110°C for specific time periods. In this study, a resin viscosity of 8cps was used in the molding of the castables containing it.

2.3. Specimens Preparation

The specimens used in the testing were molded under light vibration in the form of rectangular bars with dimensions of 25 × 25 × 150 mm.

After demolding, they were dried at 110°C for 24 hours. After drying, specimens to be used in physical and mechanical testing were sintered at 1450°C, us-

ing the firing program of Table 2, with a dwell time of 2 hours at the final temperature. On the other hand, specimens intended for dynamic elastic modulus and thermal expansion tests were only dried.

2.4. Physical and Mechanical Properties

1) The evaluated physical properties after firing at 1450˚C/2h of specimens were:
- Apparent Porosity
- Apparent Density
- Pore size distribution
- Nanoparticles dimensions and specific surface

2) The Mechanical Strength of specimens fired at 1450˚C/2h was evaluated by flexural testing in 3 point bending.

3) The Elastic Modulus versus Temperature testing of dried specimens (110˚C/24h), was evaluated by means of the impulse excitation technique, using a Resonant Frequency Damping Analyzer (RFDA-HT1600-IMCE-Belgium) in line to ASTM-1548-2 (2012). The test was conducted from room temperature to 1500˚C, under a 3˚C/minute heating rate.

4) The thermal shock testing was conducted by measuring both the residual dynamic elastic modulus, as well as the residual 3 point bending strength, after a single thermal shock test, under the sudden gradients of 300˚C, 600˚C and 1000˚C. The thermal shock was conducted by specimens cooling in running water at 24˚C.

5) The thermal expansion behavior was determined from room temperature to 1250˚C.

3. Results and Discussion

3.1. Characteristics of the Generated Alumina Nano Powder

In Table 3, the characteristic properties of the nano Alumina powder after pyrolisis and burning of the resin at 1000˚C/1h, are presented.

X-ray diffraction is a convenient method for determining the mean size of nanocrystallites in nanocrystalline bulk materials. The first scientist, Paul Scherrer, published his results in a paper that included what became known as

Table 2. Firing schedule in an electric kiln used to sinter the specimens to be used in the physical and mechanical testing.

Initial/Final Temperature (Heating Rate)	Dwell Time at the end Temperature
25˚C to 250˚C (3˚C/minute)	20 minutes
250˚C to 550˚C (3˚C/minute)	30 minutes
550˚C to 1000˚C (3˚C/minute)	30 minutes
1000˚C to 1450˚C (5˚C/minute)	120 minutes
Cooling Down (10˚C/minute)	-

Table 3. Characteristics of the nano Alumina powder generated by the burning of the resin after heat treatment at 1000°C/1h.

Specific Surface Area (BET) m²/g	86.8
Average Particle Size (nm)*	19
Crystallite Size (nm)**	15

*Calculated from the Specific Surface area. **Calculated by the Scherrer Equation.

the Scherrer equation in 1981 [1]. This can be attributed to the fact that "crystallite size" is not synonymous with "particle size", while X-Ray diffraction is sensitive to the crystallite size inside the particles. From the well-known Scherrer formula the average crystallite size, L, is:

$$L = K\lambda/\beta\cos\theta$$

where λ is the X-ray wavelength in nanometer (nm), β is the peak width of the diffraction peak profile at half maximum height resulting from small crystallite size in radians and K is a constant related to crystallite shape, normally taken as 0.9 [8].

The results confirm the nano size of the alumina powder that was generated after pyrolysis and burning of the carbon content of the liquid resin.

In **Figure 1** it can be seen that the resin indeed renders pure Al_2O_3 product after pyrolysis and oxidation starting at 900°C.

In **Figure 2** and **Figure 3** the pore size distribution and the respective cumulative porosity of the investigated castables are presented.

It can be noticed that the $ULCC_{Al_2O_3}$ castable molded with the liquid resin presented eminently pores with equivalent diameters in the range from 0.1 μm to 1.0 μm.

On the other hand, the $ULCC_{Water}$ castable molded with water presented a bigger pore size distribution range from 0.5 to 3.0 μm.

For the NCC castables, the one molded with water presented population of the pore of smaller sizes from 0.08 μm to 2.0 μm, while the $NC_{Al_2O_3}$ molded with the Al_2O_3 resin presented pore population sizes in the range from 0.1 μm to 1.0 μm.

Considering the observed range of dimensions, in all the cases, the pore sizes presented by the investigated castables, indicate a high concentration of virtually non-permeable pores to liquid metals or slag (<5 μm).

3.2. Physical Properties Results

In **Table 4** the results of Apparent Density and Apparent Porosity, after drying at 110°C/24h and after firing at 1450°C/2h, are were presented.

It can be noticed that the Apparent Densities after drying and firing are substantially bigger for the specimens containing the resin. As a consequence, the Apparent Porosity was smaller for the specimens molded with it. This fact was unexpected, considering that the samples produced using the resin as the liquid mixing vehicle, used a larger amount of molding liquid (8 wt% against 5.8 wt%
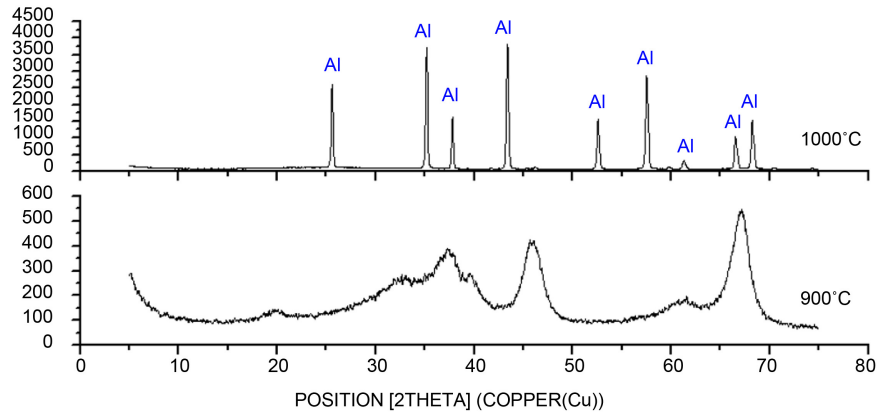
Figure 1. X-ray Diffraction patterns of the powder resulting from the heat treatment at 900˚C and 1000˚C for 1 hour of the liquid Al containing resin. Al = Al_2O_3.
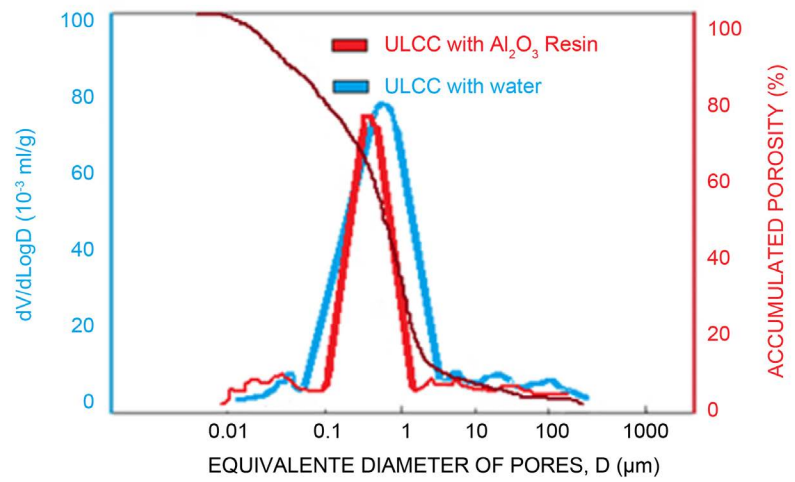

Figure 2. Pore size distribution and cumulative porosity per size of the $ULCC_{water}$ and $ULCC_{Al_2O_3}$.
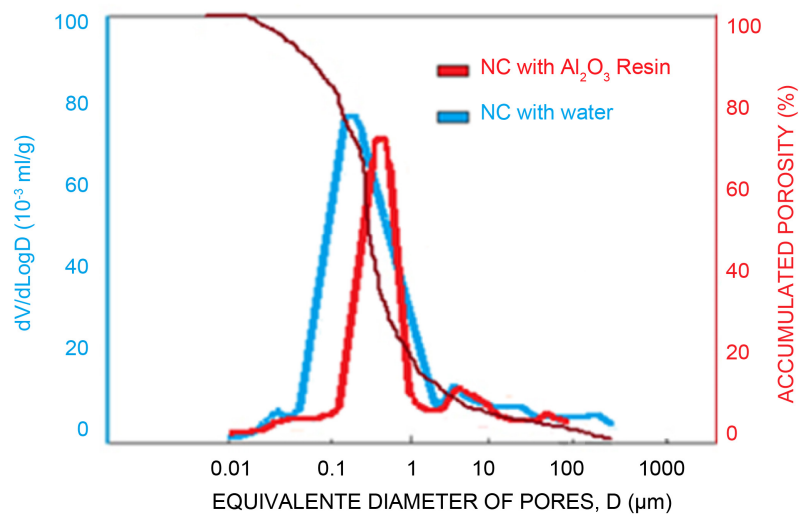

Figure 3. Pore size distribution and cumulative porosity per size of the NCC_{water} and $NCC_{Al_2O_3}$.

Table 4. Apparente Density (DA) after drying (110˚C/24h) and after firing (1450˚C/4h) and Apparent Porosity (PA) after firing (1450˚C/4h) of the castables $ULCC_{water}$, $ULCC_{Al_2O_3}$, NCC_{water} and $NCC_{Al_2O_3}$ are presented.

Composition	DA (110˚C/24h)	DA (1450˚C/4h)	PA (1450˚C/4h)
$ULCC_{water}$	2.87 g/cm^3	2.89 g/cm^3	21%
$ULCC_{Al_2O_3}$	3.02 g/cm^3	3.10 g/cm^3	18%
NCC_{water}	2.92 g/cm^3	2.98 g/cm^3	19%
$NCC_{Al_2O_3}$	3.12 g/cm^3	3.27 g/cm^3	14%

of water used in the the $ULCC_{water}$ and NCC_{water}). In addition, after firing, there was an additional mass loss because of the volatiles coming from the pyrolisis and burning of the carbon of the resin plus the eventual water excess. The results indicated a better sintered microstructure upon addition of the Al_2O_3 resin.

3.3. Results of Thermal Expansion Measurements

From **Figure 4** it can be noticed that the overall dimensional variation independent of the type of castable, including the thermal expansion coefficient (inclination of the curve), are smaller for the samples molded with the Al_2O_3 containing resin. The difference is particularly noticeable in the range from 400˚C to 900˚C. This indicates a lesser volume variation for eventual castable refractory linings molded with castables containing the Al_2O_3 resin.

In **Figures 5(a)-(c)**, the X-ray diffraction patterns of $ULCC_{Al_2O_3}$ and $NCC_{Al_2O_3}$ are presented. They explain why the castables molded with the Al_2O_3 resin displayed smaller thermal expansion coefficients. The reason resides in the fact that the aluminum oxide nanoparticles coming from the resin, reacted more readily in the aggregates environment, leading to the formation of bigger amounts of mullite ($3Al_2O_3 \cdot 2SiO_2$) and ebonite ($CaO \cdot 6Al_2O_3$) in the final phase assembly of these castables, than the castables molded only with water. This contributed to smaller thermal expansion coefficients for castables molded with the Al resin.

3.4. Results of Flexural Strength

In **Table 5** and **Figure 6**, the results of flexural strength in three-point bend, of the castables are presented. It is clear that after firing at 1450˚C/2h, the castables molded with the liquid resin presented a substantially bigger average flexural strengths than the castables molded with water. This fact indicates clearly that the nano alumina particles generated by the liquid resin were able to contribute to a much stronger castables matrices, under a microstructure condition of pores of comparable sizes and volume fraction.

3.5. Behavior of the Dynamic Elastic Modulus as a Function of the Temperature

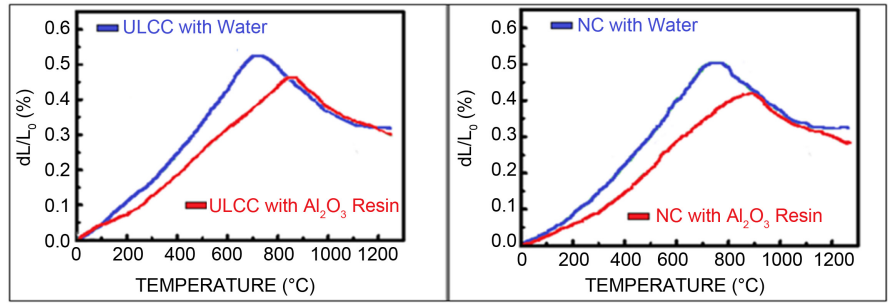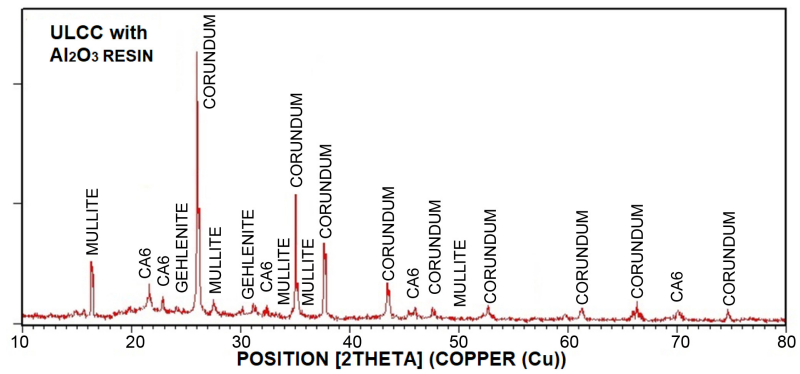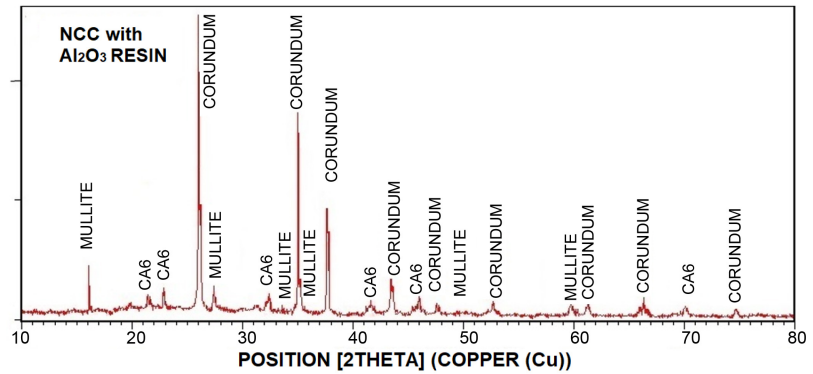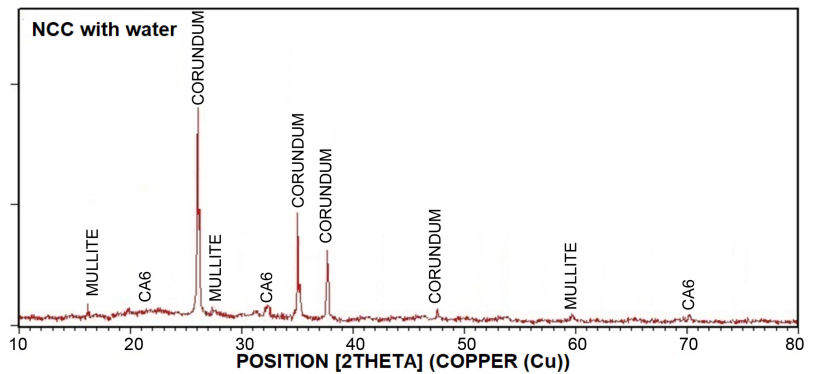The elastic modulus of ceramics upon heating to high temperatures for certain

Figure 4. Thermal Expansion measurements from room temperature to 1250°C of the dried (110°C/24h) specimens ULCC and NCC with water and Al_2O_3 Resin.

Figure 5. In (a) X-ray diffraction pattern of the $ULCC_{Al_2O_3}$. In (b) X-ray diffraction pattern of $NCC_{Al_2O_3}$. In (c) X-ray diffraction pattern of the NCC_{water}.
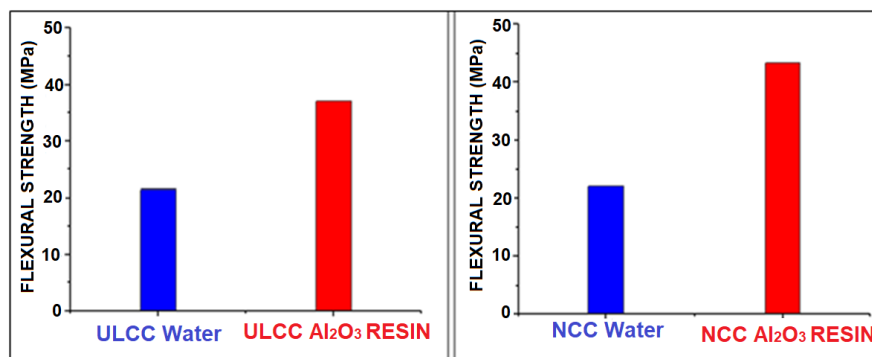
Figure 6. Flexural Strength in 3 point Bend testing of the investigated castables after firing 1450˚C/2h.

Table 5. Results of 3 Point Bend Flexural Strength of the investigated castable after firing at 1450˚C/2h.

Composition	Flexural Strength*
$ULCC_{water}$	21.5 MPa
$ULCC_{Al_2O_3}$	37.0 MPa
NC_{water}	22.2 MPa
$NC_{Al_2O_3}$	43.4 MPa

*Average over 5 specimens – standard deviations in the range ±0.3 MPa.

periods of time is sensitive to microstructure alterations caused by reactions between components, phase transitions, liquid phase development, pyroplasticity, densification (sintering) and/or defects opening.

In this work, in order to investigate the differences in microstructural evolution with the temperature of the castables, the dynamic elastic modulus of only dried specimens, was evaluated continuously from room temperature to 1450˚C, under a heating rate of 3˚C/minute. The testing was made using the impulse excitation technique IET using the equipment RFDA 1600 HT from ICEM Belgium [7] [9] [10].

The results shown in **Figure 7** and **Figure 8** indicate that similar to what happened with the flexural strength, the room temperature elastic modulus of the resin molded castables were substantially higher than those molded with water. Upon heating from room temperature to approximately 1300˚C, the elastic modulus of the castables molded with liquid resin continued to present substantially higher values of elastic modulus and display a volumetric behavior more stable than the castables molded with water.

This difference is made clearly on the respective heating up and cooling down plots as well as on the hysteresis curves, which displayed a much smaller area for the castables molded with resin. It can be seen that after cooling down, their elastic modulus at room temperature, get back very close to their initial startup value. This fact indicates that the microstructures of the castables containing resin, were less altered by a heating up and cooling down cycle, and that they
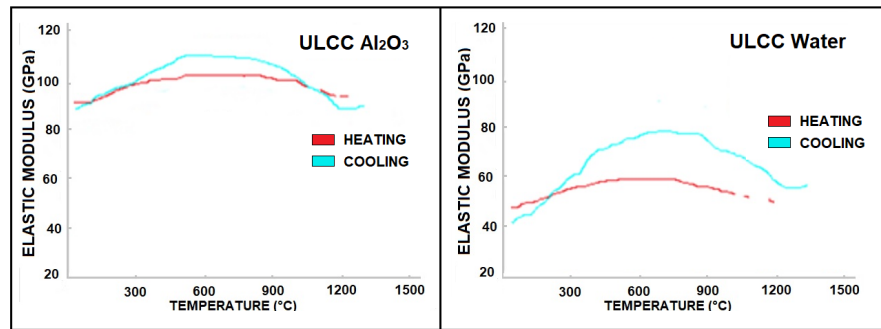
Figure 7. Elastic modulus versus temperature forcastables $ULCC_{Al_2O_3}$ and $ULCC_{water}$ dried at 110°C/24h. The heating up and cooling down rate was of 5°C/minute.
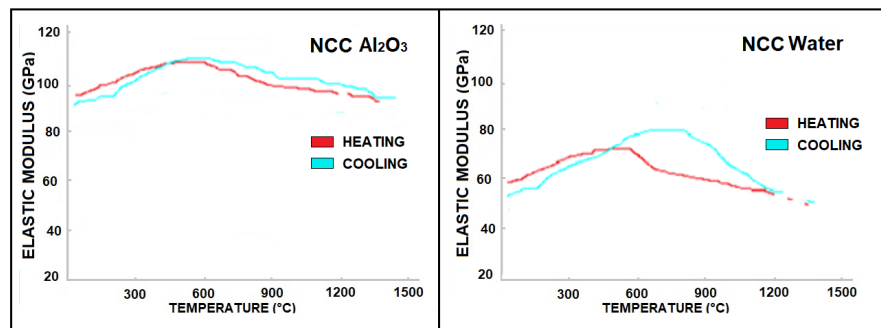

Figure 8. Elastic modulus versus temperature for castables $NCC_{Al_2O_3}$ and NCC_{water} dried at 110°C/24h. The heating up and cooling down rate was of 5°C/minute.

somewhat healed themselves from eventual defect opening upon heating and cooling, ending as strong as at the beginning of the test. Conversely, the behavior of the castables molded with water was marked by a strong hysteresis loop indicating some relevant microstructure alteration. Their elastic modulus at room temperature after the heating and cooling cycle, were still smaller than those of dried startup value, implying that just one heating up and cooling down cycle caused a reasonable level of permanent damage on their final microstructure [11].

For both castables, the ups and downs in the plots at temperatures close to 1400°C can be a credit to increasingly damping effects, caused by pyroplastic deformation originated from liquid phase development.

An examination of the cooling down plots in **Figure 7** and **Figure 8**, also indicates a slight increase of elastic modulus for both types of castables, from 1450°C down to approximately 700°C. We may credit this behavior to sintering, microstructure healing caused by the contraction of the specimens bulk phase and also to a decrease in the pyroplastic character with the hardening of the eventual liquid phase developed within the matrices of the investigated castables. Finally, from 600°C and down, the elastic modulus of both types of castables experiences a decrease (which is much bigger for the water-molded samples). This fact may indicate a possible opening of microstructure defects, caused by contraction cracking and hardening below the glass transition temperature of the

vitreous phase.

By comparing the behavior of both castables from **Figure 7** and **Figure 8**, it may then be concluded that after a firing cycle, the castables molded with the liquid resin are stronger and reached a more stable final microstructure than the castables molded with water. This is indicative of the strong sintering effect that just 1 wt% of alumina nanoparticles had in the castables matrices.

3.6. Elastic Modulus Behavior and Flexural Strength after Thermal Shock

Specimens of both castables (ULCC and NCC), with and without Al_2O_3 resin, previously fired at 1450°C/2h, were submitted to thermal shock by a single quenching in running tap water at 24°C, under the sudden gradients of 300°C, 600°C and 1000°C.

In order to evaluate the thermal shock damage, the residual elastic modulus of the shocked specimens was continuously measured from room temperature to 1450°C. In addition, the residual flexural strength after thermal shock were also determined [12] [13]. The resulting elastic modulus and residual strength versus temperature behavior after thermal shock, are shown in **Figures 9-13**.

It is evident that the first thermal shock at 300°C causes the most significant damage, displaying a fall of about 60% of the elastic modulus and flexural strength, relative to the specimens without thermal shock damage. Under the point of view of thermal shock thermo elastic theory, this temperature can be related to the critical ΔT of pure alumina materials. A second point to be observed is that the specimens with the presence of resin have a higher resistance
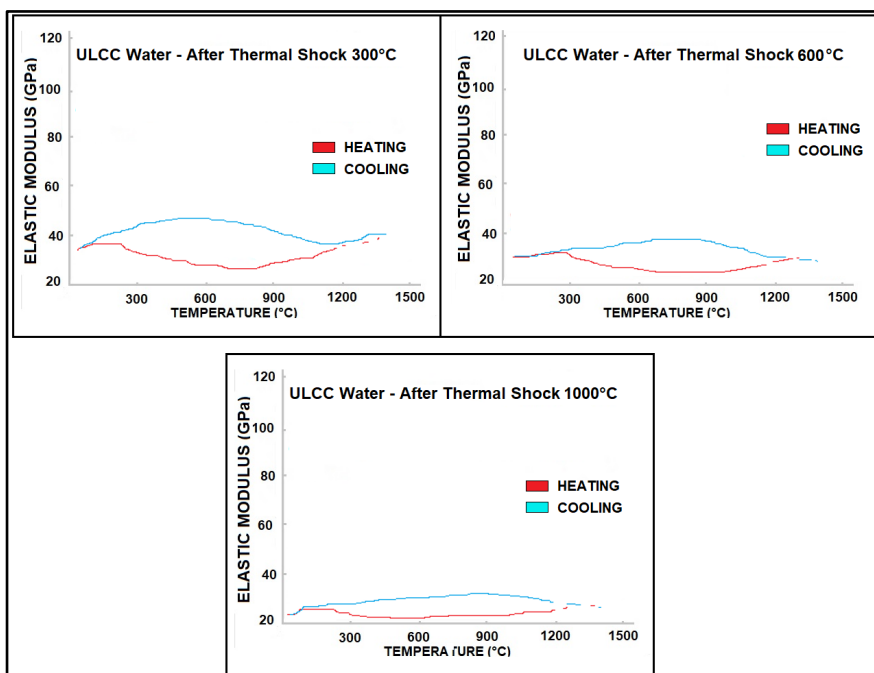

Figure 9. Residual elastic modulus versus temperature for the castable ULCC$_{water}$ pre-fired at 1450°C/2h—after thermal shock of ΔT = 300°C, 600°C and 1000°C.
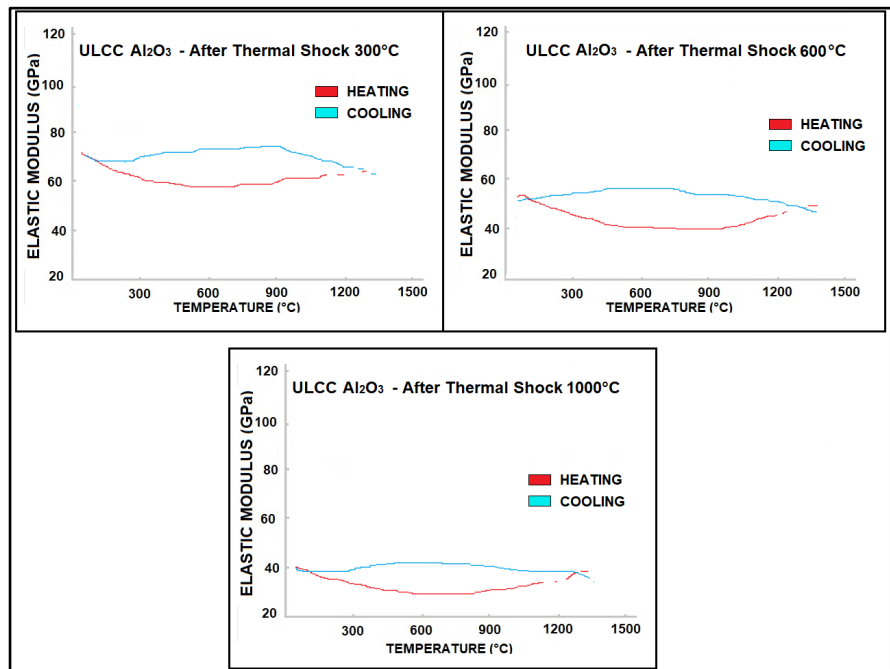
Figure 10. Residual elastic modulus versus temperature for the castable $ULCC_{Al_2O_3}$ pre-fired at 1450˚C/2h—after thermal shock of $\Delta T = 300˚C$, $600˚C$ and $1000˚C$.
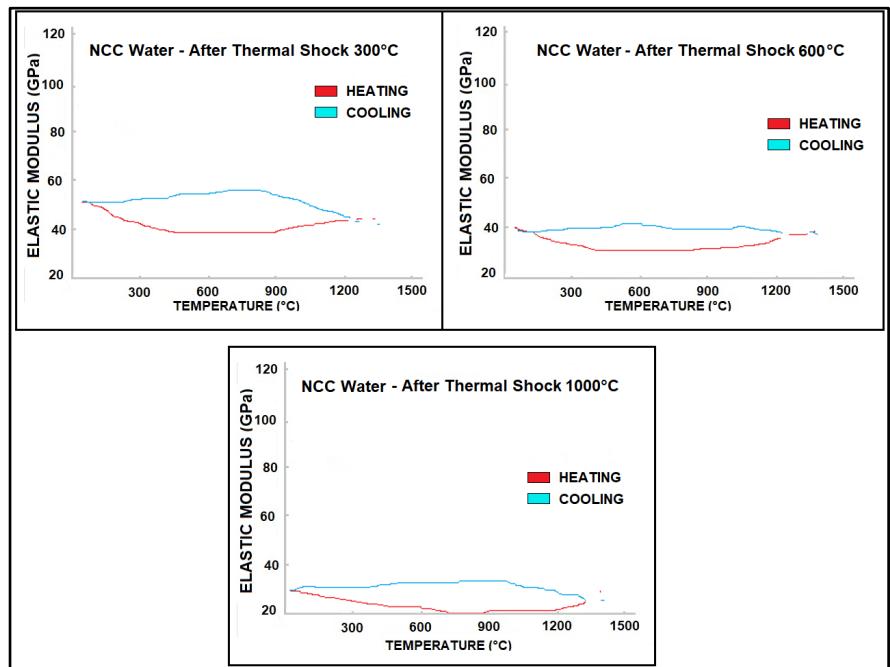

Figure 11. Residual elastic modulus versus temperature for the castable NCC_{water} pre-fired at 1450˚C/2h—after thermal shock of $\Delta T = 300˚C$, $600˚C$ and $1000˚C$.

to thermal shock damage, due to their higher final values of elastic modulus. Finally, the specimens of the ULCC type when compared to the specimens of type NCC show a better behavior against thermal shock as can be seen on its leveling off the residual flexural strength, after $\Delta T = 300˚C$.
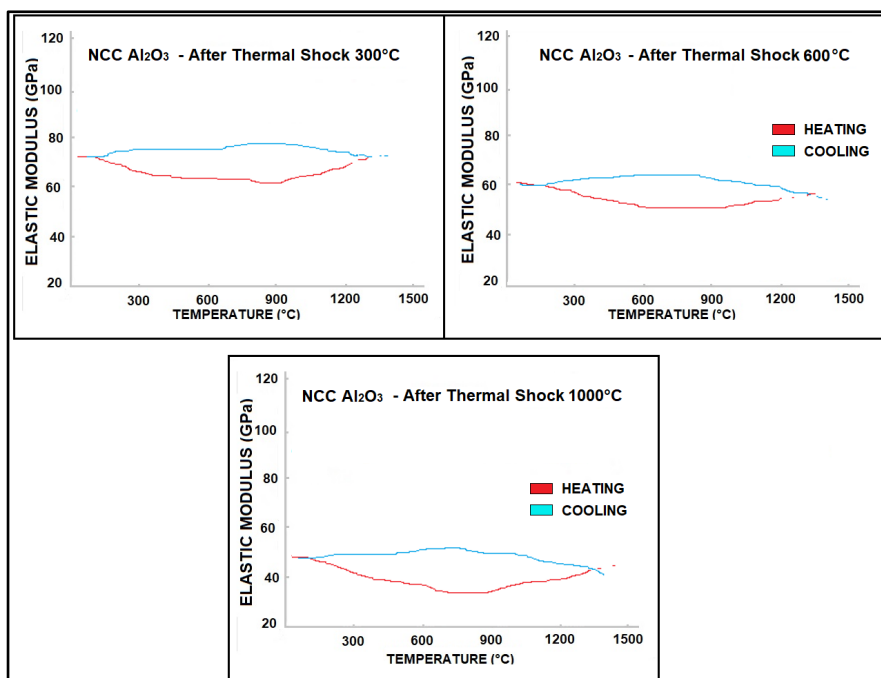
Figure 12. Residual elastic modulus versus temperature for the castable $NCC_{Al_2O_3}$ pre-fired at 1450°C/2h—after thermal shock of $\Delta T = 300°C$, $600°C$ and $1000°C$.

Figure 13. Residual flexural strength of the castables $ULCC_{Al_2O_3}$, $ULCC_{water}$, $NCC_{Al_2O_3}$ and NCC_{water}, of prefired (1450°C/2h) specimens after being submitted to a single cycle of thermal shock in running tap water at 24°C, under the temperature gradients of $\Delta T = 300°C$, $600°C$ and $1000°C$.

3.7. Comparative Test between Nano Particles Formed *in Situ* versus Nano Particles Added as a Previously Made Powder

In order to check the effectiveness of alumina nanoparticles formed *in situ* coming from the resin addition, comparatively to alumina nanoparticles added in powder form, the flexural strength and dynamic elastic modulus behavior of NCC castable in both situations were evaluated. It has to be pointed out that the addition of 8 wt% of liquid resin in the castable batch composition, results after resin pyrolisis and oxidation, on only 1 wt% of Al_2O_3 nano particles *in situ*. In this manner, a volume of liquid resin equivalent to 8 wt% of the castable's total

mass, was separately pyrolised and burnt to 1000˚C/1hour. The resulting powder was mixed in substitution of 1 wt% of the calcined reactive alumina, in the batch composition being nominated $NCC^*_{Al_2O_3}$. In this case, water was used as the mixing liquid in the amount of 5.8 wt%. The results of the flexural strength of fired specimens are shown in **Figure 14**, while the results of dynamic elastic modulus of only dried specimens are shown in **Figure 15**. It can be seen that the development *in situ* of the alumina nanoparticles coming from the resin, was
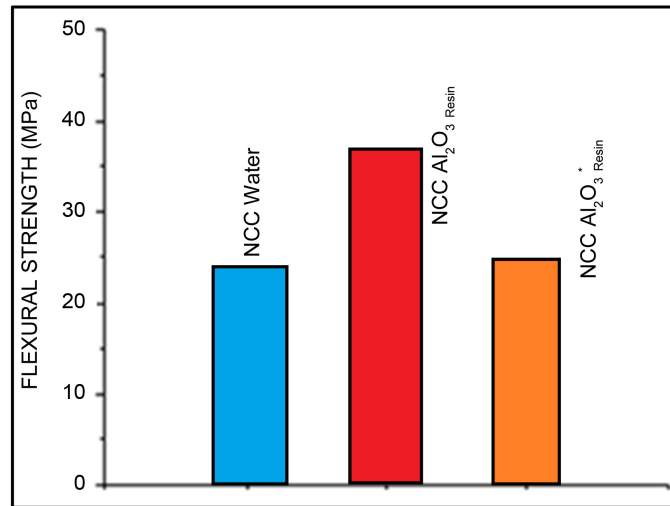

Figure 14. Flexural strength after firing at 1450˚C/2h of the NCC castablesspecimens molded only with water NCC_{water}, molded with liquid resin $NCC_{Al_2O_3Resin}$ and molded with water and containing the pyrolised resin $NCC^*_{Al_2O_3}$.
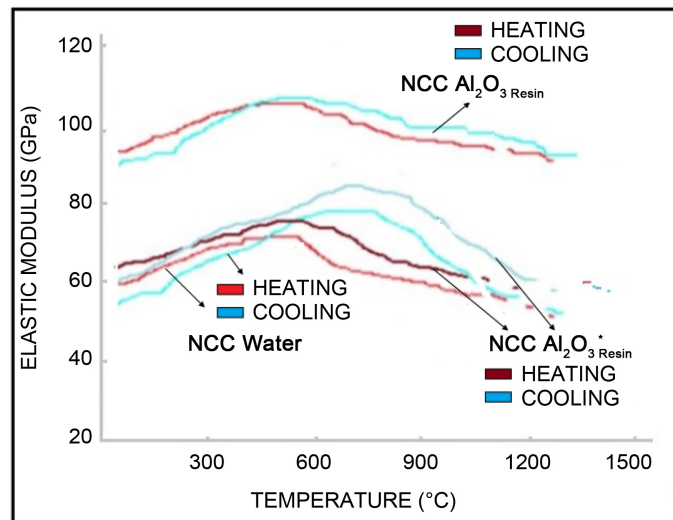

Figure 15. Dynamic elastic modulus versus temperature of test specimens just dried at 110˚C/24h, of non-cement castables; molded with liquid resin ($NCC_{Al_2O_3Resin}$) as the liquid part, molded only with water (NCC_{water}) and molded with 1 wt% of calcined resin powder ($NCC^*_{Al_2O_3}$) using water as the liquid part.

much more effective on increasing both the flexural strength and the dynamic elastic modulus, than by adding the nanoparticles in powder form. The flexural strength after the addition of the nanoparticles powder in the $NCC^*_{Al_2O_3}$, was almost the same as that of the NCC_{water} composition (without resin), showing no properties improvement at all. This fact leads to the conclusion that the development *in situ* of the alumina nanoparticles, is indeed a powerful novel route, much more effective on improving castables thermal and mechanical properties, than adding the same quantity of nanoparticles in powder form.

4. Conclusions

The results enable us to conclude that the use of a liquid aluminum carrying resin, for the development *in situ* of only 1 wt% of nano-sized alumina particles in the castables matrices, inaugurates a new very effective route in providing final microstructures much stronger and more stable, than those displayed by the castables molded with water or with the addition of an equivalent amount of nanoalumina powder. At the same time, a decrease in the thermal expansion coefficient was obtained, providing a fairly good thermal shock damage resistance.

Acknowledgements

Conflicts of Interest

The authors declare no conflicts of interest regarding the publication of this paper.

References

[1] Tomsu, F. and Palco, S. (2011) From Conventional Refractory Castables to Actual High-Quality Hydraulic Bonded Products—Development during the Last Forty Years. *International Ceramic Review*, **3**, 202-207.

[2] Bier, T.A., Bunt, E.N. and Parr, C. (1996) Calcium Aluminate Bonded Castables: Their Advantages and Applications. The Latin-American Association of Refractory Manufacturers Meeting, ALAFAR, Buenos Aires, 75-84.

[3] Funk, J.E. and Dinger, D.R. (1994) Particle Packing, Part VI—Applications of Particle Size Distribution Concepts. *International Ceramic Review*, **43**, 50-354.

[4] Badiiee, H.S. and Ostoj, S. (2011) The Effect of NanoTitania Addition on the Properties of High Alumina Low Cement Refractory Castables. *Ceramics Silikaty*, **55**, 319-325.

[5] Mukhopadhyaya, S. and Daspoddar, P.K. (2006) Role of Nanocrystalline Spinel Additive on the Properties of Low Cement Castable Refractories. *Materials and Manufacturing Processes*, **21**, 669-675. https://doi.org/10.1080/10426910600650415

[6] Pechini, M.P. (1967) Method of Preparing Lead and Alkaline Earth Titanates and Niobates and Coating Method Using the Same to form a Capacitor. US Patent No.

3330697.

[7] Gault, C. (1989) Ultrasonic Non Destructive Evaluation of Microstructural Changes and Degradation of Ceramics at High Temperature. In: Holbrook, J. and Bussiere, J., Eds., *Materials Research Society Symposium Proceedings*, Vol. 142, Materials Research Society, Pittsburgh, PA, 263-274. https://doi.org/10.1557/PROC-142-263

[8] Langford, J.I. and Wilson, A.J.C. (1978) Scherrer after Sixty Years: A Survey and Some New Results in the Determination of Crystallite Size. Journal of Applied Crystallography, **11**, 102-113. https://doi.org/10.1107/S0021889878012844

[9] Werner, J., Aneziris, C.G. and Dudczig, S. (2013) Youngs Modulus of Elasticity of Carbon Bonded Alumina Materials Up to 1450˚C. *Journal of American Ceramic Society*, **96**, 2958-2965. https://doi.org/10.1111/jace.12526

[10] Cho, T.-Y., Kim, Y.-W. and Kim, K.J. (2016) Thermal, Electrical, and Mechanical Properties of Pressureless Sintered Silicon Carbide Ceramics with Yttria-Scandia-Aluminum Nitride. *Journal of European Ceramic Society*, **36**, 2659-2665. https://doi.org/10.1016/j.jeurceramsoc.2016.04.014

[11] Brochen, E. (2011) Measuring and Modeling of Thermal Shock Resistance of Refractory Materials. Ph.D. Thesis, TU Bergakademie, Freiberg.

[12] Pereira, A.H.A., Nascimento, A.R.C. and Rodrigues, J.D.A. (2010) Effect of Non-Linearity on Young's Modulus and Damping Characterisation of High Alumina Refractory Castables Through the Impuls Excitation Technique. 53*rd International Colloquium on Refractories Aachen*, European Centre for Refractories, Germany, 90-93.

[13] Ortega, F.S., Rodrigues, J.A. and Pandolfelli, V.C. (2006) Elastic Modulus of Gelcast Cellular Ceramics at High Temperatures. *American Ceramic Society Bulletin*, **85**, 9101-9106.